Simulating the Dynamics of Polydisperse Polymer Blends: Upshot of Polydispersity and Reaction Kinetics

Gavin A. Buxton* and Nigel Clarke

Department of Chemistry, University of Durham, Durham, DH1 3LE, United Kingdom

Received June 1, 2005; Revised Manuscript Received August 9, 2005

ABSTRACT: We present a computational technique for modeling the dynamics of polydisperse polymeric systems undergoing reaction-induced phase separation. In particular, we demonstrate how the Cahn−Hilliard method, incorporating the Flory−Huggins free energy, can be used to simulate the evolution of a polydisperse−monodisperse polymer blend. To computationally model highly polydisperse polymeric systems, with constituents ranging from monomers to linear chains comprised of 10^5 segments, we suitably discretize the molecular weight distribution. We demonstrate how our reduced component scheme does not affect the general polymer blend dynamics, before using our approach to elucidate the effects of polydispersity on the dynamics of such systems. In this manner, the complex dynamics of phase separation between polymers of different species and the interdiffusion between polymers of different lengths are accurately captured. Furthermore, we couple our model of polymer blend dynamics with Flory−Stockmayer reaction kinetics and simulate the dynamics of reaction-induced phase separation in polymer blends. We demonstrate that the behavior of such systems is sensitive not only to the complex interplay between enthalpy and entropy but also to entanglement effects between polymers of increasing lengths.

I. Introduction

Polymers are versatile and have been widely utilized in a variety of everyday applications. This is, in part, due to the fact that the physical and chemical properties of polymers can be tailored by varying the length and chemical composition of the polymer chains. Furthermore, different polymer materials can be mixed together during processing to create polymer blends, which offer material scientists the opportunity to control and finely tune the macroscopic properties of the polymeric material.[1] However, different polymer species are often immiscible and phase separate upon blending, and this can have a detrimental effect on the macroscopic properties of the polymeric material.[2] Furthermore, polymers are often polydisperse (polymer chains are of different lengths), and therefore, the polymer blend phase separates not only due to chemical differences between the species but also due to differences in the entropy of mixing between small and large polymer chains.[3]

It has been observed (both theoretically and experimentally) that larger, and more cumbersome, chains are confined into the center of the phase-separated domains while the smaller chains, which have a greater translational entropy, are allowed to diffuse into neighboring domains.[3,4] In other words, the distribution of chain lengths in polydisperse polymers is *not* spatially uniform, subsequent to phase separation. Therefore, during the dynamics of polymer blend evolution not only is the concentration fluctuations of the different polymer species evolving, but there is also a complex interplay between the mobility and thermodynamics of polymers of different lengths. This phenomenon is also important when elucidating the dynamics of reaction-induced phase separation, a process whereby polymers of increasing lengths, polydispersity, and immiscibility are created via in situ chemical reactions.[5,6]

Reaction-induced phase separation essentially occurs by transferring the polymer blend from the one-phase region into the two-phase region by increasing the degree of polymerization of the polymer. The binary mixture is initially homogeneous, but as the length of the polymer chains increases (via polymerization), the system becomes increasingly unstable and phase separation occurs. This is an important mechanism for controlling both the structure and the physical properties of the polymer mixture through reaction kinetics.[5]

Here we elucidate the complex dynamical behavior of polydisperse systems and, in particular, the complex interplay between phase separation and polymerization in reaction-induced phase separation. We use the Cahn−Hilliard theory modified for polydisperse polymeric systems to model the dynamics of phase separation in polymer blends. Furthermore, we include a description of the reaction kinetics of polymerization using the Flory−Stockmayer theory. In this manner we simulate the evolution of a polymer blend subject to reaction kinetics.

The Cahn−Hilliard method is a phenomenological model for capturing the diffusive nature of phase separation in binary mixtures.[7,8] However, this model can be extended to quantitatively capture the behavior of polymeric systems and, in particular, account for chain connectivity. The Flory−Huggins theory can be chosen as the local energy contribution which dictates the equilibrium mixing concentrations,[9,10] while the square gradient energy term can be extended to account for the entropic effects of chain connectivity.[11] Furthermore, the Flory−Huggins formulation can be extended to polydisperse mixtures.[10] The Flory−Huggins theory for polydisperse mixtures involves a summation over all degrees of polymerization, essentially treating polymers of different lengths as if they were separate polymeric species. This can result in a large number of separate components (on the order of 10^5 for linear polymers) which is computationally intractable. It is therefore necessary to obtain an alternative description for the free energy of polydisperse systems which involves the evolution of fewer parameters, or components.

10.1021/ma051136q CCC: $30.25
Published on Web 09/20/2005

Schichtel and Binder[12] analytically modeled the early-stage dynamics of phase separation in a polydisperse system, considering the polymer mobility to be dictated by the presence of "vacancies". Huang and de la Cruz[13] later considered the phase separation dynamics in polydisperse−monodisperse polymer systems, without such an assumption. Although the polydispersity was restricted to one-, two-, and three-component representations, this enabled a weight-average degree of polymerization and a polydispersity index to be obtained. This approach was extended by Clarke[14] to account for an *arbitrary* number of components using a matrix formulation and led to the analytical investigation of fluctuation growth rates, following a quench into the two-phase region.

Alternatively, a reduced moment description of the free energy has recently been introduced, which can allow the late-stage dynamics of phase separation to be captured. Here the large number of components that represent the full polydispersity are replaced by a few moments of the size distribution.[15,16] This methodology has been used to analyze the equilibrium phase behavior of polydisperse polymer blends and has recently been extended to the dynamics of phase separation. In particular, Warren[17] considered the dynamics for the overall density (collective diffusion) to be faster than the dynamics of the moments (self-diffusion). The early stages of phase separation have also been investigated analytically by Pagonabarraga and Cates[18] where not only did they consider length polydispersity (in a manner analogously to Clarke[14]) but also chemical polydispersity, where the enthalpic interaction strengths varied continuously. Since our work focuses on the behavior of composition variations too large to be described by linearized equations of motion, our results are not directly comparable with the work of ref 18. Yashin and Balazs[19] introduced a method for capturing the dynamics of the first moments of the molecular weight distribution (volume fraction and concentration). Their method enabled the dynamics of interdiffusion to be captured in a polydisperse system. However, there is still uncertainty considering the dynamics of reduced moment systems as no attempt to compare such systems with alternative methods has been made.

In the current investigation we adopt the approach of Huang and de la Cruz[13] and Clarke[14] in order to model the evolution of a finite number of components. In particular, we take advantage of the $1/N$ dependence in both the free energy of mixing and the polymer chain mobility (for entangled chains) and represent the full range of polydispersity with a finite number of components via an exponentially increasing coarse-grained representation. That is, components of similar degrees of polymerization are "grouped together", and the range over which this grouping occurs increases with increasing degree of polymerization. This enables us to capture the dynamics of a polydisperse system with a reduced number of components, while not having to adopt a reduced moment description.

In section II we detail the methodology we employ to simulate the evolution of a polydisperse−monodisperse system. Furthermore, we show how this system can be solved in tandem with Flory−Stockmayer kinetics to capture the complex dynamics of reaction-induced phase separation. In section III we compare the evolution of our reduced component system with that of a full component system and use our reduced component methodology to investigate the effects of polydispersity and polymerization on the phase separation dynamics in polymer blends. Finally, we summarize our results and draw relevant conclusions.

II. Methodology

The methodology presented in this paper is for a mixture of polydisperse polymer A and monodisperse polymer B. The volume fraction of the ith component of polymer A is denoted by ϕ_{Ai}, and its degree of polymerization is denoted by N_{Ai}. Likewise, the volume fraction and degree of polymerization of polymer B are denoted by ϕ_B and N_B, respectively. We consider the mixture to be incompressible and force the volume fractions to obey the constraint $\phi_A + \phi_B = 1$ (for brevity we define $\phi_A = \sum_i \phi_{Ai}$). The local free energy of mixing for this mixture is given by the Flory−Huggins theory,[10] including a square gradient term which introduces energetic costs to gradients in the concentrations:[11,12]

$$\frac{F}{k_\beta T} = \int_v \sum_i \frac{\phi_{Ai}(\mathbf{r})}{N_{Ai}} \ln \phi_{Ai}(\mathbf{r}) + \frac{\phi_B(\mathbf{r})}{N_B} \ln \phi_B(\mathbf{r}) + \chi \sum_i \phi_{Ai}(\mathbf{r})\, \phi_B(\mathbf{r}) + \frac{b^2}{36} \sum_n \frac{(\nabla \phi_n)^2}{\phi_n} \mathrm{d}\mathbf{r} \quad (1)$$

k_β is the Boltzmann constant, T is the temperature, χ is the Flory−Huggins enthalpic interaction parameter, and b is the statistical length of a "Kuhn" segment. The integral is performed over the volume, V, of the sample. The summation, $\sum_i$, is over all components of polymer A while the summation, $\sum_n$, is over all polymer components. In the remainder of the paper we set $k_\beta T = 1$ for convenience. The local terms of the free energy can produce an energy minimum in the intermixed region ($\phi_A \approx \phi_B \approx 0.5$) for low degrees of polymerization and low χ-parameter. As either the degree of polymerization or the χ-parameter is increased, this local term produces two minima: one in which the polymer is A-rich ($\phi_A > 0.5$) and one in which the polymer is B-rich ($\phi_B > 0.5$). This is enough to establish the equilibrium phase behavior: however, to establish interfacial dynamics and drive domain coarsening, the square gradient term must be included. This gradient term describes the energy necessary to create an interface between homogeneous domains. We note that in ref 20 Pagonabarraga and Cates proposed a different free energy functional for polydisperse polymers, which reduces to eq 1 when expanded in gradients of the compositions, and only the lowest order gradient terms are retained. A comparison of the effects of these different free energy functionals on the dynamics is beyond the scope of the present study, but particularly in the case of strong segregation and sharp interfaces, it may be interesting to consider the consequences of utilizing the theory of ref 20.

To drive polymer blend dynamics, we must first consider the chemical potentials in the system. (It should be noted that matter flows spontaneously from a region of high chemical potential to a region of low chemical potential.) The chemical potential in a polydisperse mixture is generally related to the free energy by

$$\mu_m = F + \sum_n (\delta_{mn} - \phi_n) \frac{\partial F}{\partial \phi_n} \quad (2)$$

where the summation is over all components (A-polymer and B-polymer) and δ_{mn} is the Dirac delta function. It is, however, more convenient to consider the difference in chemical potential between an A-polymer component and the B-polymer component

$$\mu_{Ai} - \mu_B = \frac{\partial F}{\partial \phi_{Ai}} - \frac{\partial F}{\partial \phi_B} \tag{3}$$

Considering the chemical potential in this form significantly simplifies the expressions.[12,14] The derivatives of the free energy with respect to the volume fraction of either a component of A-polymer or the B-polymer component (obtained directly from eq 1) are given by

$$\frac{\partial F}{\partial \phi_{Ai}} = \frac{1 + \ln \phi_{Ai}}{N_{Ai}} + \chi\phi_B - \frac{b^2}{36}\left[\frac{2\nabla^2\phi_{Ai}}{\phi_{Ai}} + \frac{(\nabla\phi_{Ai})^2}{{\phi_{Ai}}^2}\right]$$

$$\frac{\partial F}{\partial \phi_B} = \frac{1 + \ln \phi_B}{N_B} + \chi\phi_A - \frac{b^2}{36}\left[\frac{2\nabla^2\phi_B}{\phi_B} + \frac{(\nabla\phi_B)^2}{{\phi_B}^2}\right] \tag{4}$$

Having established the free energy (and resultant chemical potentials), we now turn our attention to the dynamics of this model.

The starting point to describing the dynamics of polymer interdiffusion and phase separation is the continuity equation (ensuring conservation of mass)

$$\frac{\partial \phi_m}{\partial t} = -\nabla \cdot \mathbf{J}_m \tag{5}$$

where $\mathbf{J}_m$ is the flux of the mth component. The flux can be written as the sum of the local flux that would occur in a fixed background and the flux due to a common flow field, v_m (i.e., common to all polymer components but still defined locally).[14] The former contribution is assumed to be proportional to the gradient of the chemical potential of a given component, resulting in a flux of the form $J_m = \lambda_m \nabla\mu_m + \phi_m v_m$. This flux can be conveniently rewritten in terms of the difference in chemical potential as

$$\mathbf{J}_i = \sum_j \Lambda_{ij} \nabla(\mu_j - \mu_B) \tag{6}$$

where the summation is over all A-polymer components and Λ_{ij} are the Onsager coefficients describing the interdiffusion of polymer chains.[21] It has been shown that the Onsager coefficients are given by[14]

$$\Lambda_{ij} = (\delta_{ij} - \phi_i)\lambda_j - \phi_j\lambda_i + \phi_i\phi_j \sum_m \lambda_m \tag{7}$$

where the summation is over all polymer components and λ_m is the mobility of the mth polymer component. It should be noted that the Onsager coefficients are symmetric, thus ensuring a reciprocal relationship between flows and forces of different polymer components. The mobility of polymer chains exhibits a transition in behavior as a function of the degree of polymerization. For smaller chains ($N < N_e$, where N_e is the threshold for entanglement) the mobility is proportional to the monomer−monomer friction coefficient, λ_{0m}. For longer chains, however, entanglement effects can play an influential part in the mobility of the chains, and the mobility is found to be inversely proportional to the degree of polymerization according to the tube model. Thus, the mobility of the polymer chains is given by[22]

$$\lambda_m = \begin{cases} \phi_m\lambda_{0m} & (N < N_e) \\ \phi_m\lambda_{0m}\dfrac{N_e}{N_m} & (N \geq N_e) \end{cases} \tag{8}$$

For simplicity, we assume that the monomer−monomer friction coefficient, λ_{0m}, is the same for all polymer species and independent of ϕ.

The above set of equations describe the diffusive nature of polymer blend dynamics for a polydisperse system and can be directly solved using a finite-difference scheme.[23,24] However, to capture polydispersity effects, all chain lengths must, in general, be treated as separate polymer components. Thus, a system containing on the order of 10^5 components would be required to capture the dynamics of a typical polydisperse linear polymer material. This is computationally unfeasible, and therefore, we select a reduced number of components that can still capture the behavior of this system. Our approach takes into consideration the $1/N$ dependence within both the free energy of mixing term and the mobility of the polymer chains (at least for entangled chains). That is, for very small chains ($1 \leq N \leq 9$) the $1/N$ dependence is large, and it is inappropriate to attempt to coarsen the polymer size distribution. However, for slightly larger chains ($10 \leq N \leq 99$) we may coarsen the size distribution into groups of 10 (e.g., the polymer components of size $10 \rightarrow 19$ are represented by a single component of length $N = 14.5$). We can extend this argument further: chains of length $100 \leq N \leq 999$ are coarsened into groups of 100 (e.g., the polymer components of size $100 \rightarrow 199$ are represented by a single component of length $N = 149.5$). This argument can be extended to increasing degrees of polymerization (chains of length $1000 \leq N \leq 9999$ and $10000 \leq N \leq 99999$ are coarsened into groups of 1000 and 10000, respectively). In this manner we can capture the dynamics of a highly polydisperse system, where N varies from 1 (monomer) through to 10^5, with only 45 components (nine components per order of magnitude in polymer chain length). In the next section we will demonstrate how such a reduced component scheme adequately captures the dynamics of a full component system.

We are interested in capturing not only the dynamic behavior of a polydisperse blend but also the reaction kinetics of in situ polymerization. We consider the polymerization kinetics to be described by the Flory−Stockmayer theory.[25,10] All unreacted functional groups are considered to be equally reactive (except intramolecular reactions which are prohibited). It should be noted that breakup processes are not considered in the current model. The evolutionary equations for Flory−Stockmayer reaction kinetics, due to random reactions between pairs of linear polymers, are given by[25,10]

$$\frac{1}{C}\frac{\partial M_i}{\partial t} = 2\sum_{j=1}^{j=i-1} M_j M_{i-j} - 4M_i \sum_{j=1}^{j=N-i} M_j \tag{9}$$

where M_i is the number of i-mers (polymeric molecules composed of i units) and C is the bimolecular rate constant. The first term on the right-hand side of eq 9 describes the formation of i-mers from polymers of shorter lengths, while the second term accounts for the consumption of i-mers through the creation of longer

polymers. If the number of i-mers is given by M_i, then the volume fraction of i-mers is proportional to N_iM_i; hence, the total volume fraction of A-like polymers is proportional to $\sum_i N_iM_i$.

To apply these reaction kinetics to our reduced component scheme, we rewrite eq 9 in terms of averaged quantities

$$\frac{\partial\langle M_i\rangle}{\partial t} = C\sum_{j,k} K_{ijk}\langle M_j\rangle\langle M_k\rangle \tag{10}$$

where $\langle M_i\rangle$ represents the average number of polymers over a discrete grouping. For example, $\langle M_{14.5}\rangle$ represents the average number of polymers whose sizes lie between $N = 10$ and $N = 19$. K_{ijk} is a $45 \times 45 \times 45$ lookup matrix of reaction coefficients which dictates the reaction kinetics. This enables us to account for the reaction kinetics between 45 separate components. The coefficients, K_{ijk}, are directly obtained by replacing the full distribution in eq 9 with averaged quantities. For example, if M_{17} appears in eq 9, then this is replaced by $\langle M_{14.5}\rangle\langle N_{14.5}\rangle/N_{17}$ when appearing in eq 10 (recall that the polymer components of size $10 \rightarrow 19$ are represented by a single component of length $N = 14.5$). This means that varying the concentration of a given i-mer in eq 9 is represented by an appropriate increase in concentration of an averaged quantity in eq 10. The concentrations are normalized by the ratio of degree of polymerization in order to ensure that mass is neither created nor destroyed during the reaction. This allows us to capture the Flory−Stockmayer reaction kinetics in our reduced component scheme, while conserving mass.

We now demonstrate how our reduced component scheme compares to a full component system, before presenting results exhibiting the models ability to capture the dynamics of polydisperse polymer blends and simulate reaction-induced phase separation.

III. Results and Discussion

This section presents results and relevant discussions concerning (i) the comparison between results obtained from our reduced component scheme and those obtained from solving the full distribution, (ii) the effects of polydispersity and the overall shape of the molecular weight distribution, (iii) phase separation in polydisperse−monodisperse systems, and (iv) the kinetics of reaction-induced phase separation.

A. Discretization Effects. We compare a system consisting of a reduced component molecular weight distribution to a system containing the full distribution. Because of the computational expense of solving a system consisting of the full distribution, we limit the current analysis to polymer chain lengths between monomers and $N = 99$. We consider a system where the degree of polymerization of the monodisperse B polymer is $N_B = 50$ and the average concentrations of all polydisperse A polymer components are the same. This ensures that the weight-averaged degree of polymerization, $\bar{N}_{Aw} = (\sum_i \phi_{Ai}N_{Ai})/\phi_A$, is equal to 50. To compare the dynamics between a system containing a reduced number of components (only 18 components are required to capture the polydispersity of this system) and the full distribution, we consider the incipient dynamics of a dissolving interface between two homogeneous regions. The system is of length $L = 128$, and the average concentration of A-polymer is $\phi_{A0} = 0.5$. The interface is described by the equation $\phi_A(x,0) = {}^1/_2\{1 - \phi_{A0}\tanh[\delta_0(x - L/2)]\}$, where δ_0 controls the width of the interface (this is currently set to unity). No flux boundary conditions are enforced at $x = 0, L$ (all gradients are assumed to be zero, such that there is no net flow across the simulation boundaries). The χ-parameter is set to 0.001, and the system is evolved with a time step of $\Delta t = 0.001$.

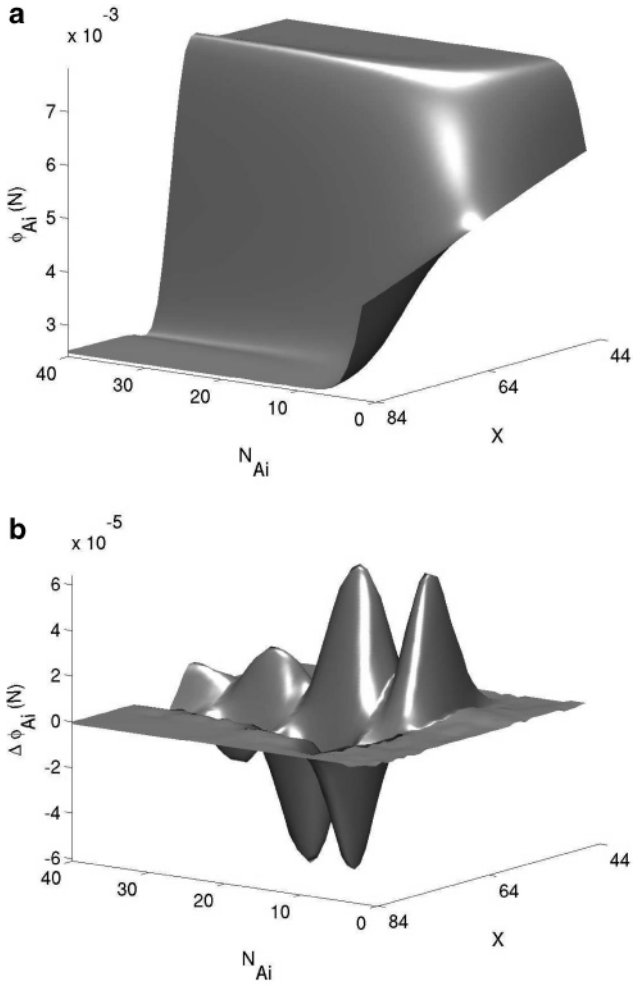

Figure 1. Two-dimensional profiles of (a) polymer A concentrations for the full component system and (b) difference in concentration between the full component solution and the reduced component solution, as a function of position, x, and degree of polymerization, N_{Ai}.

Figure 1 shows the concentrations for the full component system at time $t = 10^6\Delta t$, along with the concentration difference between the full and reduced component systems. The concentration profile as a function of N and x (note only the interfacial area of interest is shown) for the full component system is depicted in Figure 1a. The interfacial region at $x = 64$ is clearly observed at higher values of N, however, for low values of N the interfacial structure is almost completely dissolved. The decreased energy of mixing and the higher chain mobilities are both responsible for the relatively fast dissolution of the interfacial structure for low molecular weight chains.

Discretization effects are highlighted in Figure 1b, which depicts the difference in concentration between the full component solution and the reduced component solution. The concentration in the reduced component system is obtained from linear interpolation between the averaged values of N. This can be seen as the relatively large differences (on the order of 1%, com-

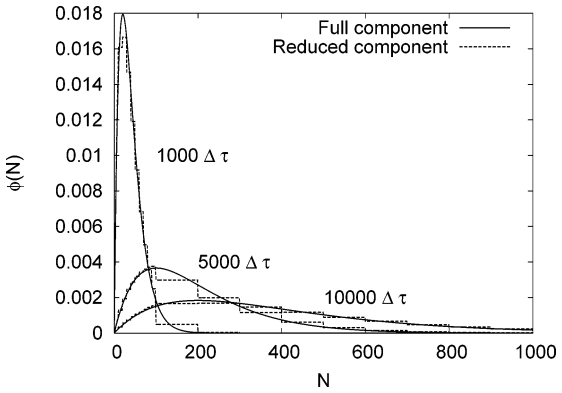

Figure 2. Concentration of polymer as a function of the degree of polymerization at various times during the reaction. We contrast the evolution of systems employing the full component solution and our reduced component scheme.

pared to values in Figure 1a) in regions where linear interpolation is performed. However, there would appear to be no difference in the dynamics in the low N region ($N < 10$) between the full component solution and the reduced component solution. Furthermore, the difference between the two systems goes to essentially zero in the center of the groupings (that is, $N = 14.5$, 24.5, 34.5, etc.). This means that the reduced component system accurately captures the polymer blend dynamics at the exact values of N at which the average quantities are evolved. It would also imply that averaging the contribution from groups of N does not significantly alter the general dynamics of the system.

We also consider the effects of our reduced component scheme on the reaction kinetics of linear polymerization (see eqs 9 and 10). Figure 2 shows the concentration as a function of the degree of polymerization at various times during the reaction. We contrast the evolution of systems employing the full component solution (see eq 9) and our reduced component scheme (see eq 10). The results from the reduced component system are shown as "steps" where the height of the step is the average concentration and the width of the step represents the region of N over which the averaging is performed. Given the large discretization effects, the two solutions are clearly very close, and the reaction kinetics are seen to be qualitatively conserved.

B. Polydispersity and Molecular Weight Distribution. To assess the effects of polydispersity on the dynamics of a polymer blend, and the effects of molecular weight distribution in general, we simulate the dynamics of a polymer blend where the molecular weight of one of the components is described by a Gaussian distribution. In this manner, we can vary the standard deviation of this distribution and assess the effects of increasing polydispersity. Furthermore, we contrast systems containing a unimodal and bimodal molecular weight distribution, both of which possess the same weight-average degree of polymerization and polydispersity index (polydispersity index, I_P, is defined as the ratio between the weight-averaged and number-averaged degrees of polymerization).

We consider the dissolution of an initial perturbation in the polymer concentrations. In particular, we introduce a domain of A-rich polymer and B-rich polymer by assigning a sinusoidal concentration profile and follow the dissolution of this initial perturbation with time. The simulations are of size $L = 100$ with periodic boundary conditions, and the temporal and spatial

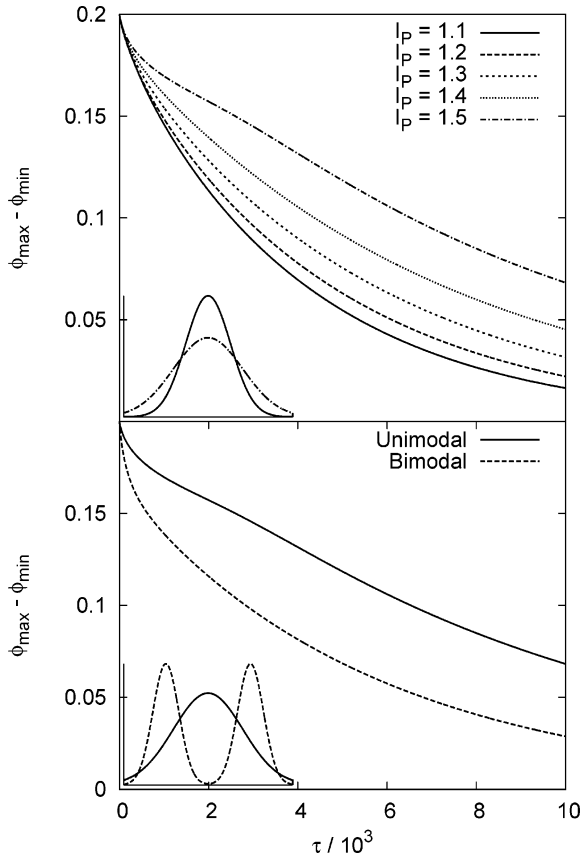

Figure 3. Evolution of the difference between the maximum and minimum values of ϕ_A as a function of time. Molecular weight distributions are also depicted in the bottom left-hand corner of both plots.

discretizations are $\Delta\tau = 0.001$ and $\Delta x = 0.25$, respectively. The molecular weight distribution is described by $\phi_A(N) \propto \exp(-W(N - 500)^2)$, where we vary W in order to vary the polydispersity; the bimodal distribution is obtained from the superposition of two unimodal distributions (of equal variance) centered at $N = 250$ and $N = 750$. Here, we select the degree of polymerization of polymer B and the weight-averaged degree of polymerization of polymer A to be the same (i.e., $\bar{N}_{Aw} = N_B = 500$). We evolve the system at a χ-parameter of 0.003, which is less than the critical χ-parameter of 0.004.

Figure 3 shows the evolution of the difference between the maximum and minimum values of ϕ_A as a function of time. Initially, the difference between the extreme values in the initial concentration perturbation is 0.2. However, as the structure dissolves toward a homogeneous solution, the difference between the maximum and minimum values of ϕ_A becomes significantly reduced. In the upper plot of Figure 3 we consider the effects of polydispersity by varying the polydispersity index, I_P, from 1.1 to 1.5, while the lower plot contrasts systems containing unimodal and bimodal distributions (I_P is 1.5 for both systems). The molecular weight distributions of these systems are also depicted in the bottom left-hand corner of both plots. In the upper plot it can be seen that increasing the polydispersity index slows down the dissolution process; the difference between the maximum and minimum values of ϕ_A is larger for the more polydisperse systems. The lower plot shows that the system containing a bimodal molecular weight distribution evolves much faster then the system containing a unimodal distribution. It should be noted

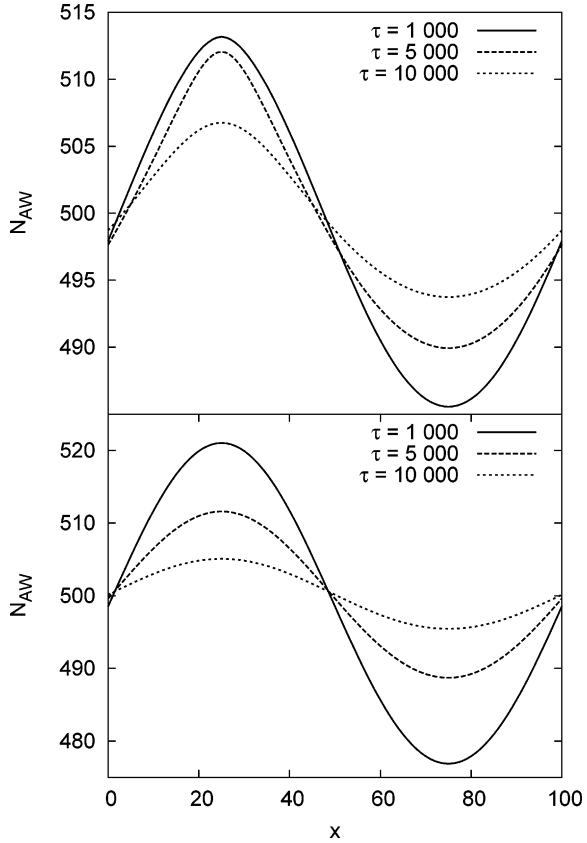

Figure 4. Profiles of the weight-averaged degree of polymerization at different times. The upper plot exhibits profiles for the unimodal case (polydispersity index of 1.5) while the lower plot shows profiles for the equivalent bimodal case.

that dissolution in the bimodal case occurs much quicker in the first peak ($N = 250$) of the molecular weight distribution.

To understand these trends, we consider profiles of the weight-averaged degree of polymerization at different times in Figure 4. The upper plot exhibits profiles for the unimodal case (polydispersity index of 1.5) while the lower plot shows profiles for the equivalent bimodal case. Initially, the fields are uniform with respect to the molecular weight distributions, and only the concentration profiles are nonuniform. However, as the system relaxes toward the equilibrium homogeneous profile, the low molecular weight material is capable of relaxing faster than the high molecular weight material. This results in the rapid diffusion of low molecular weight material from the A-rich domain to the B-rich domain, and hence, the weight-averaged degree of polymerization is higher in the A-rich phase and lower in the B-rich phase (i.e., the sinusoidal concentration profile is reflected in the molecular weight distribution). This can be seen in Figure 4 at the early stage ($\tau = 1000$) of the simulation, prior to the gradual dissolution of the remaining structure through the diffusion of higher molecular weight material. In other words, the low molecular weight material evolves much quicker than the high molecular weight material, and this results in the dissolution of the structure at early times for the low molecular weight material. The system then evolves through the gradual diffusion of the high molecular weight material in a system where the driving force for dissolution is significantly reduced due to the homogenized low molecular weight profile. Therefore, while the diffusion of low molecular weight material controls

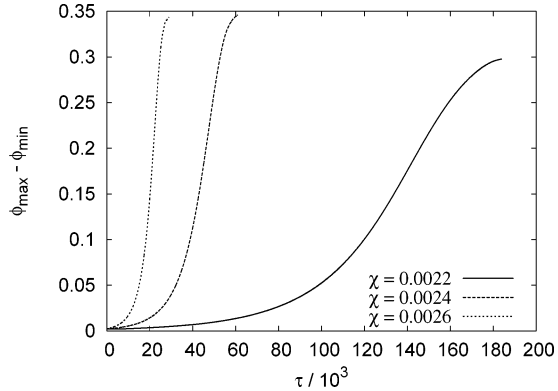

Figure 5. Evolution of the difference between the maximum and minimum values of ϕ_A as a function of time. Systems evolved under different χ-parameters are contrasted.

the initial stages of the dissolution dynamics, the late stages are dominated by the diffusion of the high molecular weight material. This results in the relatively slow dynamics of the systems of higher polydispersity; a greater amount of highly localized high molecular weight material remains in the center of the A-rich domains, resulting in a sharp peak in the $\bar{N}_{Aw}$ profile (see upper plot of Figure 4). Furthermore, this can be seen in the relatively fast dissolution of the system containing the bimodal molecular weight distribution and, in particular, the larger variations in $\bar{N}_{Aw}$ at early times as the low molecular weight peak ($N = 250$) of the bimodal distribution rapidly diffuses from the A-rich phase to the B-rich phase.

C. Monodisperse−Polydisperse Polymer Blend. We now turn our attention to the phase separation dynamics of a monodisperse−polydisperse mixture. The molecular weight distribution for the polydisperse component is obtained from Flory−Stockmayer reaction kinetics, thereby providing a realistic distribution of molecular sizes (see distributions in Figure 2). A weight-averaged degree of polymerization of $\bar{N}_{Aw} = 1000$ is obtained, and the degree of polymerization for the monodisperse B polymer is $N_B = 1000$. We start from an initially perturbed system where the average initial concentration is $\phi_{A0} = 0.5$. This initial condition is obtained by performing a moving average over a Gaussian distributed order parameter (of mean 0.001) and results in a random, yet smooth, small-amplitude starting configuration. This results in a critical χ-parameter of $\chi_s = 0.002$; we, therefore, consider the phase separation kinetics for systems of increasing the χ-parameter above this critical value. We solve these systems using a time step of $\Delta\tau = 0.025$ and spatial step of $\Delta x = 0.25$.

Figure 5 shows the evolution of the difference between the maximum and minimum values of ϕ_A as a function of time. We consider the evolution of three systems corresponding to χ-parameters of 0.0022, 0.0024, and 0.0026. (It should be noted that at $\chi = \chi_s = 0.002$ concentration fluctuations decrease and no phase separation occurs.) The effect of increasing χ is to cause phase separation to occur earlier in the simulation.

The concentration profiles for two systems ($\chi = 0.0022$ and $\chi = 0.0026$) are shown in Figure 6. The upper plot of Figure 6 depicts the concentration profiles at various times during phase separation in the system where $\chi = 0.0022$, while the lower plot shows the concentration profiles for the system where $\chi = 0.0026$. The main difference is the increased number of domains that form in the system of larger χ-parameter. This is a conse-

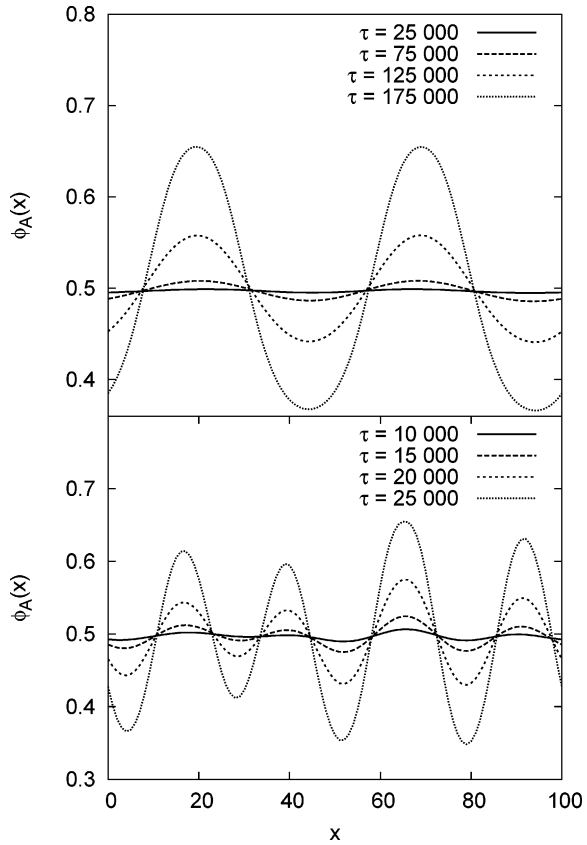

Figure 6. Concentration profiles at various times during phase separation in systems where $\chi = 0.0022$ (upper plot) and $\chi = 0.0026$ (lower plot).

quence of the time over which phase separation occurs. As would be expected in monodisperse systems, the system where $\chi = 0.22$ takes longer to phase separate than the system where $\chi = 0.0026$, due to a lower energy of mixing. Prior to phase separation, the gradient term of the free energy dominates and the initial perturbations become gradually smoother; hence, the longer the system evolves prior to phase separation the larger the emergent domain structures. It should be noted that the domain sizes are expected to grow with time in all the systems considered here; for numerical reasons, however, we limit the present study to the incipient dynamics of phase separation.

We now consider the spatial reorganisation of smaller and larger chains in the polydisperse system. Figure 7 depicts the weight-averaged degree of polymerization and the polydispersity index for the system with $\chi = 0.0022$ at various times. The upper plot depicts $\bar{N}_{\mathrm{Aw}}$ and reveals that not only is there spatial variations in $\bar{N}_{\mathrm{Aw}}$, but that these variations correlate to the domains in the upper plot of Figure 6. Furthermore, the lower plot (which shows the polydispersity index) reveals the formation of lower polydispersity in the B-domains and higher polydispersity in the A-domains. From this we can ascertain that the larger molecular weight material is confined into the A-domain while the lower molecular weight material is allowed to diffuse into neighboring domains. Both high and low molecular weight materials are present in the A-domain, increasing I_{P} relative to that in the B-domain, where the A polymer material is predominantly of low molecular weight. This can be contrasted with the same information, but provided for the system where $\chi = 0.0026$, depicted in Figure 8. Again, we see that the higher molecular weight material

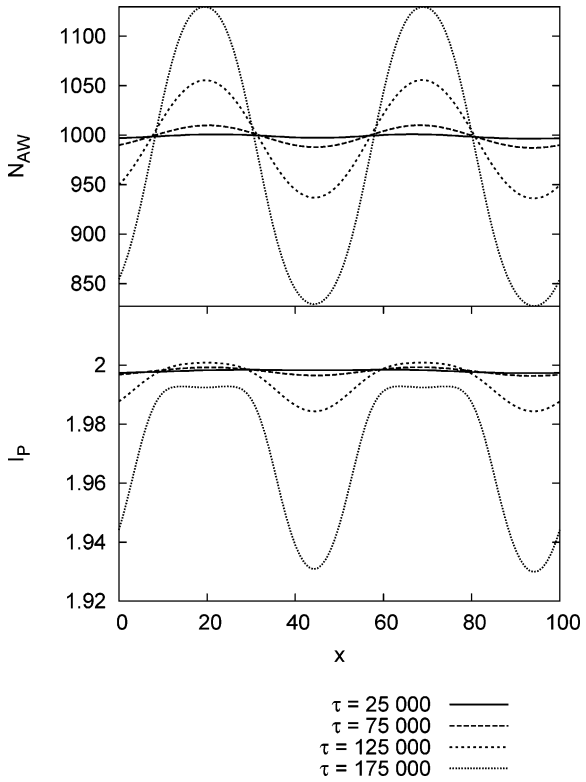

Figure 7. Weight-averaged degree of polymerization (upper plot) and the polydispersity index (lower plot) for the system with $\chi = 0.0022$ at various times.

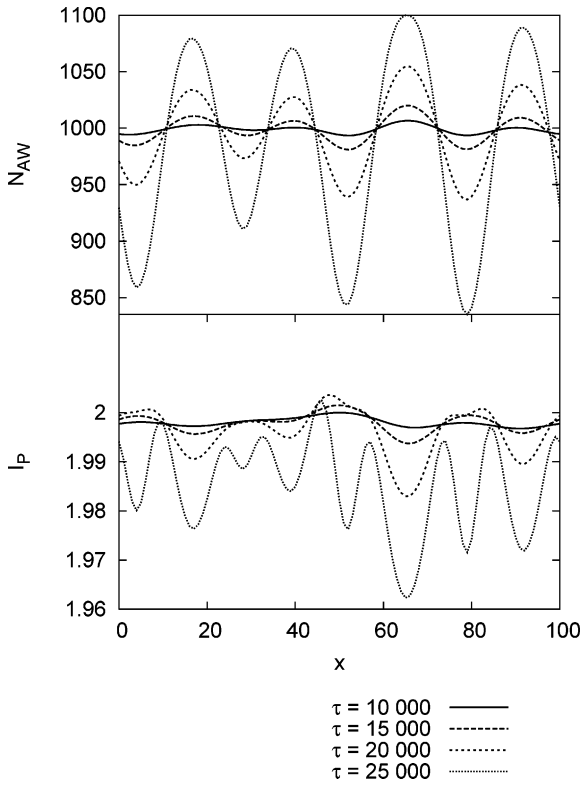

Figure 8. Weight-averaged degree of polymerization (upper plot) and the polydispersity index (lower plot) for the system with $\chi = 0.0026$ at various times.

is located primarily in the A-phase of the phase-separated structure. Now, however, the polydispersity shows a smaller variation and is larger at the interface and smaller in both the A- and B-domains. This implies that in this highly dynamic system the distributions of

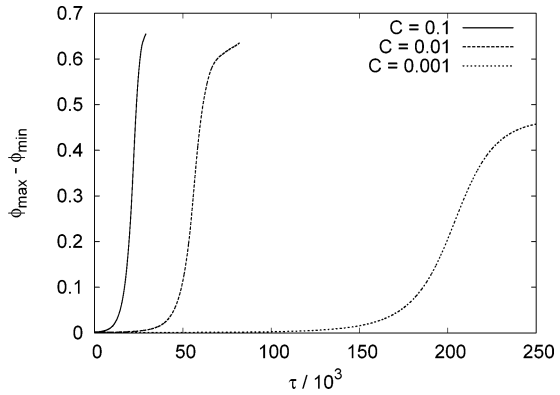

Figure 9. Evolution of the difference between the maximum and minimum values of ϕ_A as a function of time. Systems evolved under different reaction rates are contrasted.

molecular weight are much broader at the interface than in either the A- or B-rich domains.

D. Reaction-Induced Phase Separation. We now simulate phase separation in a polymer blend induced, not by an increase in χ-parameter, but by an increase in the degree of polymerization via reactive polymerization. Similar to before, we begin with a weight-averaged degree of polymerization of $\bar{N}_{Aw} = 1000$ and a degree of polymerization for the monodisperse B polymer of $N_B = 1000$. We start from an initially perturbed system where the average initial concentration is $\phi_{A0} = 0.5$, and hence, the critical χ-parameter is $\chi_s = 0.002$. However, instead of increasing the χ-parameter above this value and allowing the system to evolve (and ultimately phase separate), we allow the system to evolve at $\chi = \chi_s$ and instead introduce reaction kinetics.

Figure 9 depicts the difference between the maximum and minimum values of ϕ_A as a function of time for various systems undergoing reaction-induced phase separation. We consider bimolecular reaction rate constants of $C = 0.001$, $C = 0.01$, and $C = 0.1$ (see eqs 9 and 10) and in this manner capture a wide range of reaction kinetics. Phase separation is found to occur sooner in systems with higher reaction rates, as would be expected considering that the degree of polymerization (and, hence, entropy of mixing) in the A polymer increases faster with higher reaction rates.

The composition profiles for the systems with reaction rates of $C = 0.001$ and $C = 0.1$ are considered in Figure 10. The upper plot depicts the composition for the system with a reaction rate of $C = 0.001$ while the system depicted in the lower plot possesses a reaction rate of $C = 0.1$. Systems of increasing reaction rate are shown to phase separate faster, and hence, the emergent structure tends to have smaller domains. This is analogous to the systems depicted in Figure 6, where the systems phase separated faster due to a higher χ-parameter. However, the mechanism by which initial concentration fluctuations are smoothed prior to phase separation are the same. The longer the system takes prior to phase separation, the more that the gradient term can reduce interfacial tension by smoothing the initial concentration perturbations and, hence, larger domain sizes emerge. It should also be noted that the systems appear to be asymmetric with the A-rich regions being slightly broader than the B-rich regions. In particular, the concentration peaks in the A-rich phase appear "flattened".

The weight-average degree of polymerization, along with the polydispersity index, is considered in Figure

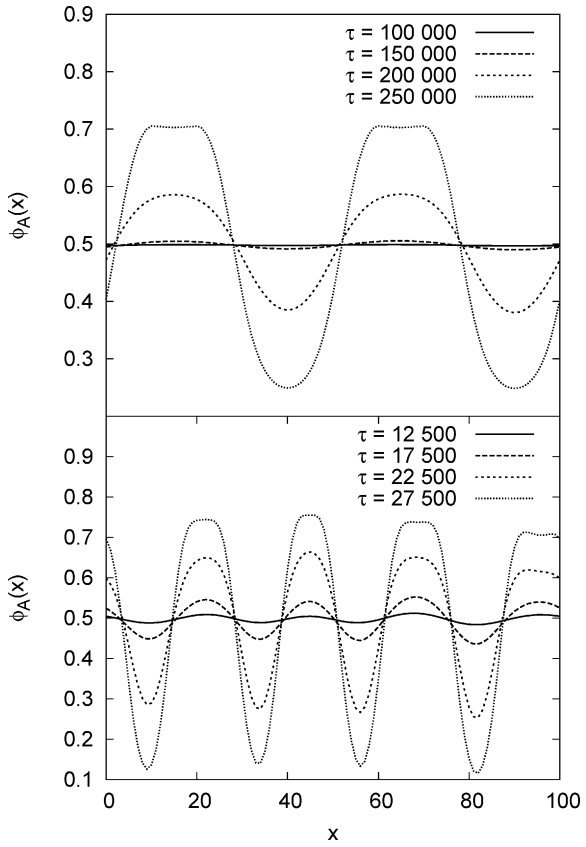

Figure 10. Concentration profiles at various times during phase separation in systems where $C = 0.001$ (upper plot) and $C = 0.1$ (lower plot).

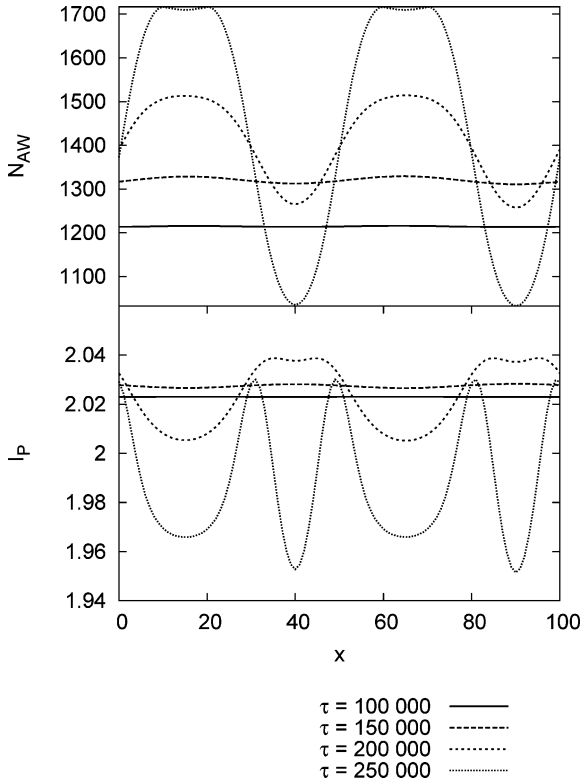

Figure 11. Weight-averaged degree of polymerization (upper plot) and the polydispersity index (lower plot) for the system with $C = 0.001$ at various times.

11 for the system with $C = 0.001$. There is a gradual increase in $\bar{N}_{Aw}$ with time (upper plot of Figure 11) due to the gradual increase in degree of polymerization

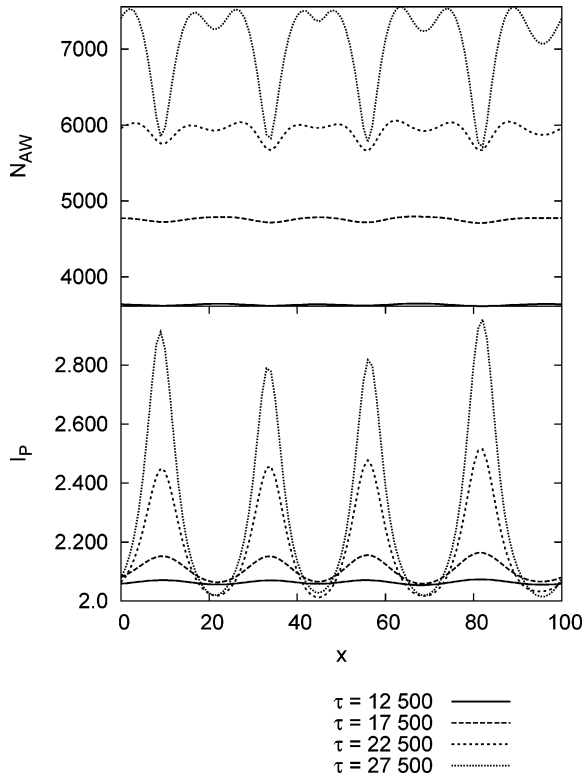

Figure 12. Weight-averaged degree of polymerization (upper plot) and the polydispersity index (lower plot) for the system with $C = 0.1$ at various times.

caused by the reaction kinetics. Furthermore, the system exhibits a significant variation in $\bar{N}_{Aw}$ which corresponds with the regions of A-rich polymer that form during the reaction-induced phase separation. The lower plot of Figure 11 depicts the polydispersity index of the same system. There is a reduction in the polydispersity index in both the A-rich and B-rich domains, with an increase occurring at the interface. This, along with the significant variations in the weight-average degree of polymerization, leads to the conclusion that there is polymer chain segregation as a function of the chain size. The smaller chains are present in both the A-rich and B-rich phases, while the larger chains are located primarily in the A-rich phase. It should also be noted that larger chains will react to form increasingly larger chains, and therefore, the in situ reaction kinetics are likely to accentuate this trend.

The weight-average degree of polymerization, along with the polydispersity index, is considered in Figure 12 for the system with $C = 0.1$. The faster reaction rate causes a more rapid increase in the degree of polymerization as shown in the upper plot of Figure 12. Again, the structure of $\bar{N}_{Aw}$ follows that of the A polymer concentrations; however, the peaks of the $\bar{N}_{Aw}$ profile appear as doublets, or "twin peaks". These twin peaks are a direct consequence of the complex dynamics of phase separation during reactive polymerization. The lower plot of Figure 12 shows the polydispersity index for this system at various times. Interestingly, the polydispersity index exhibits large values in the center of the B-rich phase. This is due to the presence of small amounts of both shorter and longer chains in the B phase, while in the A phase there are small amounts of shorter chains but a large amount of longer chains.

To gain additional insight into this dynamic behavior, we present the two-dimensional concentration profiles

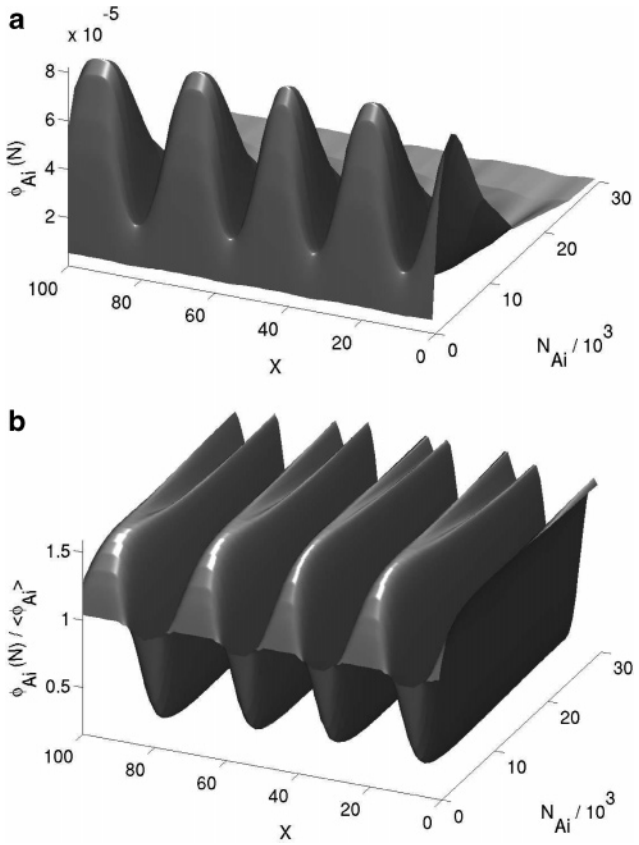

Figure 13. Two-dimensional profiles of (a) polymer A concentrations and (b) normalized polymer A concentrations, as a function of position, x, and degree of polymerization, N_{Ai}.

(ϕ_{Ai}) as a function of molecular weight in Figure 13a. The concentrations reveal an increase at $N_{Ai} \approx 7000$ (which corresponds with $\bar{N}_{Aw}$ in Figure 12). The phase-separated structure is also clearly evident in the concentration profiles, as a function of x. However, the twin peaks observed in $\bar{N}_{Aw}$ are not evident in the concentration profile. To see how the twin peaks are formed, we plot the relative concentration profiles in Figure 13b; that is, $\phi_{Ai}(N)/\langle\phi_{Ai}\rangle$, where $\langle\phi_{Ai}\rangle$ is averaged over x. These relative distributions enable the low and high molecular weight concentration profiles to be clearly seen—regions where the magnitudes of the concentrations were small in Figure 13a. The low molecular weight material shows an almost homogeneous distribution, with just as much low molecular weight material being present in the B-rich domains as in the A-rich domains. The high molecular weight material, however, not only reveals the phase-separated structure but also the formation of the twin peaks observed in Figure 12. At equilibrium the high molecular weight material would be expected to localize in the center of the A-rich domains; however, this is a system not at equilibrium. The migration of A-like polymer chains of increasing molecular weight toward the center of the A-rich domains is moderated by the low mobility of these long chains. This results in the inability of the larger chains to diffuse to the center of the A-rich domains during the time taken for phase separation to occur, and hence, regions of high molecular weight material are found at the edges of the A-rich domains.

IV. Summary and Conclusions

In this paper, we show how the dynamics of polydisperse−monodisperse polymer blends and Flory−Stock-

mayer polymerization reaction kinetics can be combined to simulate reaction-induced phase separation. In particular, the polydispersity is represented using a "reduced component" scheme which is shown to correctly capture both the dynamics of a polydisperse polymer blend and the kinetics of in situ reactive polymerization.

We use our reduced component scheme to contrast the dynamics of polymer blends where one of the species has differing polydispersity and molecular weight distribution. Both the polydispersity of the polymer and the molecular weight distribution have a significant effect on the dynamics of these system; interesting dynamic behavior derives from the complex interplay between enthalpy (polymers of different species) and entropy (polymers of different molecular weights). In particular, we show that the dynamics of a polydisperse−monodisperse polymer blend are different for unimodal and bimodal molecular weight distributions, of equal polydispersity index and weight-averaged degree of polymerization. Thus, the physics of polydisperse polymer systems cannot necessarily be captured by representing the molecular weight distribution by its first couple of moments.

Also, we elucidate the incipient phase separation dynamics in polydisperse−monodisperse polymer blends after a quench into the two-phase region. As expected, domains are formed, rich in either A-like or B-like polymer. Furthermore, not only does phase separation occur between different polymer species but also spatial segregation ensues between polymers of different sizes. We find size segregation in the polydisperse A polymer, such that low molecular weight material is dispersed throughout the sample, while high molecular weight material becomes more localized in the center of the A-phase (this is consistent with previous theoretical[3] and experimental[4] studies).

Finally, reaction-induced phase separation is simulated by thrusting a polymer blend from the one-phase region into the two phase region via reactive polymerization. The complex dynamics of phase separation between polymers of different species, and interdiffusion between polymers of different lengths, are captured in these systems. Entanglement effects are found to be increasingly influential on the dynamic behavior of reaction-induced phase separation. In particular, increasingly immobile polymer chains are formed as the degree of polymerization is increased. This is found to result in the inability of very high molecular weight chains to migrate to the center of the A-rich phase during the time scale of phase separation.

In conclusion, we have shown how phase separation dynamics of polydisperse polymer blends can be computationally coupled with Flory−Stockmayer reaction kinetics to yield a model capable of capturing the dynamics of reaction-induced phase separation in polymer blends. It should be noted, however, that the current model neglects hydrodynamic effects and assumes the polymer dynamics to be entirely diffusive. Despite this simplification, a wealth of interesting dynamical behavior is observed, and the results presented here offer key insights into the fundamental physics of reaction-induced phase separation. Furthermore, it is expected that the approach presented in this paper will offer a benchmark with which to validate the dynamics of models incorporating a reduced moment description of the polymer polydispersity.

References and Notes

(1) Paul, D. R.; Bucknall, C. B. In *Polymer Blends*; Wiley: New York, 2000.
(2) Sperling, L. H. In *Polymeric Multicomponent Materials*; Wiley-Interscience: New York, 1997.
(3) Broseta, D.; Fredrickson, G. H.; Helfand, E.; Leibler, L. *Macromolecules* **1990**, *23*, 132.
(4) Nam, K. H.; Jo, W. H. *Polymer* **1995**, *36*, 3727.
(5) Inoue, T. *Prog. Polym. Sci.* **1995**, *20*, 119.
(6) Alig, I.; Rüllmann, M.; Holst, M.; Xu, J. *Macromol. Symp.* **2003**, *198*, 245.
(7) Cahn, J. W.; Hilliard, J. E. *J. Chem. Phys.* **1958**, *28*, 258.
(8) Cahn, J. W. *J. Chem. Phys.* **1965**, *42*, 93.
(9) Huggins, M. L. *J. Am. Chem. Soc.* **1942**, *64*, 1712.
(10) Flory, P. J. In *Principles of Polymer Chemistry*; Cornell University Press: Ithaca, NY, 1953.
(11) de Gennes, P. G. *J. Chem. Phys.* **1980**, *72*, 4756.
(12) Schichtel, T. E.; Binder, K. *Macromolecules* **1987**, *20*, 1671.
(13) Huang, C.; Olvera de la Cruz, M. *Macromolecules* **1994**, *27*, 4231.
(14) Clarke, N. *Eur. Phys. J. E* **2001**, *4*, 327.
(15) Warren, P. B. *Phys. Rev. Lett.* **1998**, *80*, 1369.
(16) Sollich, P.; Cates, M. E. *Phys. Rev. Lett.* **1998**, *80*, 1365.
(17) Warren, P. B. *Phys. Chem. Chem. Phys.* **1999**, *1*, 2197.
(18) Pagonabarraga, I.; Cates, M. E. *Macromolecules* **2003**, *36*, 934.
(19) Yashin, V. V.; Balazs, A. C. *J. Chem. Phys.* **2004**, *121*, 2833.
(20) Pagonabarraga, I.; Cates, M. E. *Europhys. Lett.* **2001**, *55*, 348.
(21) Following Clarke,[14] $\mathbf{J}_m = \lambda_m \nabla\mu_m + \phi_m v_m$ is rewritten as $\mathbf{J}_m = \lambda_m \nabla\mu_m - \phi_m \sum_n \lambda_n \nabla\mu_n$, which allows us to write $\mathbf{J}_i = \sum_i \delta_{ij}\lambda_j \nabla\mu_j - \phi_i \sum_j \lambda_j \nabla\mu_j - \phi_i \lambda_B \nabla\mu_B$. Taking into consideration the Gibbs−Duhem relation $\sum_n \phi_n \nabla\mu_n = 0$, the flux can be written as $\mathbf{J}_i = \sum_j (\delta_{ij}\lambda_j - \phi_i\lambda_j + g_i\phi_j)\nabla\mu_j - (\phi_i\lambda_B - g_i\phi_B)\nabla\mu_B$, which considering the expression for the Onsager coefficients in eq 7, and taking $g_i = \phi_i\lambda_B + \sum_j(\phi_i - \delta_{ij})\lambda_j$, results in the expression for $\mathbf{J}_i$ given in eq 6.
(22) Brochard, F.; Jouffroy, J.; Levinson, P. *Macromolecules* **1983**, *16*, 1638.
(23) Zhang, H.; Zhang, J.; Yang, Y. *Macromol. Theory Simul.* **1995**, *4*, 1001.
(24) Glotzer, S. C. *Annu. Rev. Comput. Phys.* **1995**, *2*, 1.
(25) Stockmayer, W. H. *J. Chem. Phys.* **1943**, *11*, 45.

MA051136Q